Extremely efficient internal exciton dissociation through edge states in layered 2D perovskites

Jean-Christophe Blancon, Hsinhan Tsai, Wanyi Nie, Constantinos C Stoumpos, Laurent Pedesseau, Claudine Katan, Mikaël Kepenekian, Chan Myae Myae Soe, Kannatassen Appavoo, Matthew y Sfeir, et al.

Extremely efficient internal exciton dissociation through edge states in layered 2D perovskites

J.-C. Blancon,[1] H. Tsai,[1,2] W. Nie,[1] C. C. Stoumpos,[3] L. Pedesseau,[4] C. Katan,[5] M. Kepenekian,[5] C. M. M. Soe,[3] K. Appavoo,[6] M. Y. Sfeir,[6] S. Tretiak,[1] P. M. Ajayan,[2] M. G. Kanatzidis,[3,7] J. Even,[4] J. J. Crochet,[1]* A. D. Mohite[1]*

[1]Los Alamos National Laboratory, Los Alamos, NM 87545, USA. [2]Department of Materials Science and Nanoengineering, Rice University, Houston, TX 77005, USA. [3]Department of Chemistry, Northwestern University, Evanston, IL 60208, USA. [4]Fonctions Optiques pour les Technologies de l'Information (FOTON), INSA de Rennes, CNRS, UMR 6082, 35708 Rennes, France. [5]Institut des Sciences Chimiques de Rennes (ISCR), Université de Rennes 1, CNRS, UMR 6226, 35042 Rennes, France. [6]Center for Functional Nanomaterials, Brookhaven National Laboratory, Upton, NY 11973, USA. [7]Department of Materials Science and Engineering, Northwestern University, Evanston, IL 60208, USA.

*Corresponding author. Email: jcrochet@lanl.gov (J.C.C.); amohite@lanl.gov (A.D.M.)

Understanding and controlling charge and energy flow in state-of-the-art semiconductor quantum-wells has enabled high-efficiency optoelectronic devices. Two-dimensional Ruddlesden-Popper perovskites are solution-processed quantum-wells wherein the band gap can be tuned by varying the perovskite layer thickness, which modulates the effective electron-hole confinement. We report that, counterintuitive to classical quantum-confined systems where photo-generated electrons and holes are strongly bound by Coulomb interactions or excitons, the photo-physics of thin films made of Ruddlesden-Popper perovskites with a thickness exceeding two perovskite crystal-units (>1.3 nanometers) is dominated by lower energy states associated with the local intrinsic electronic structure of the edges of the perovskite layers. These states provide a direct pathway for dissociating excitons into longer-lived free-carriers that significantly improve the performance of optoelectronic devices.

Two-dimensional (2D) Ruddlesden-Popper perovskites (RPPs) are a class of quantum-well (QW) like materials described by the formula $A_nA'_{n-1}M_nX_{3n+1}$ where A, A' are cations, M is metal and X is halide; the value of n determines the QW thickness and, as a result, the degree of quantum and dielectric confinement as well as the optical band gap (or color) (*1–9*). They have emerged as an alternative to bulk (3D) organic-inorganic (hybrid) perovskites because of their technologically relevant photo- and chemical-stability coupled with high-performance optoelectronic devices (*10–12*). Compared with 3D perovskites and classical semiconductor-based QWs, RPPs offer tremendous advantages because of the tunability of their optoelectronic properties through both chemical and quantum-mechanical degrees of freedom. For two decades, most RPP crystals with n=1 (*6*, *13–15*) have been studied with few prototypes of optoelectronic devices (*3*, *16*). Recently, the synthesis of phase-pure (purified to one n-value) 2D perovskites with high n-values (n=2 to 5) was achieved (*4*), which led to the demonstration of high-efficiency thin film solar cells based on RPPs n=3,4 with technology-relevant stability (*12*). However, there is limited understanding of the fundamental physical properties of phase-pure 2D perovskites of high n-value in thin films typically used for optoelectronic applications. Furthermore, the fate of photogenerated electron-hole pairs and the underlying photophysical processes such as charge separation and recombination are unknown.

We investigated photophysical and optoelectronic properties of phase-pure homogenous 2D perovskites, and show that in thin films (fig. S1) for n>2, there exists an intrinsic mechanism for dissociation of the strongly bound electron-hole pairs (excitons) to long-lived free-carriers provided by lower energy states at the edges of the layered perovskites. Moreover, once carriers are trapped in these edge states, they remain protected and do not lose their energy via non-radiative processes and can contribute to photocurrent in a photovoltaic (PV) device or radiatively recombine efficiently as desired for light-emission applications. We validate these findings through PV devices with record efficiencies and two-orders higher photoluminescence quantum yields (PLQY) using n>2 layered perovskites.

The crystal structure and evidence for phase-purity of the investigated layered 2D perovskite family of $(BA)_2(MA)_{n-1}Pb_nI_{3n+1}$ with n from 1 to 5 are shown in Fig. 1, A and B. In order to understand the origin of the thin film optical properties, we compared them to those of their exfoliated crystal counterparts prepared by mechanically exfoliating few-layers of pristine RPPs crystals. The optical absorption and photoluminescence (PL) properties of the thin films and exfoliated crystals are illustrated Fig. 1, C to F (fig. S1) (*17*), along with bulk $CH_3NH_3PbI_3$ perovskites for comparison.

There was a dramatic difference in the optical properties of the thin films and exfoliated crystals (Fig. 1, C to H, and table S1 and fig. S2) (*17*). In the exfoliated crystals, band gap

absorption and emission increased monotonously from 1.85 eV to 2.42 eV with decreasing n from 5 to 1 (QW thickness varying from 3.139 nm to 0.641 nm), which is expected from quantum and dielectric confinement resulting in many-body interactions and large exciton binding energies at room temperature (*5–9*, *13*, *18*). This behavior was confirmed by estimating the exciton binding energies as a function of n (figs. S3 and S4) (*17*), which amounts to 380 meV, 270 meV, and an average value of 220 meV for n=1, n=2 and n>2, respectively. These values of exciton binding energy (>200 meV) attest to the robustness of the excitonic states at room temperature in phase pure RPPs up to n=5. They are about one order of magnitude larger than the values found in 3D lead halide perovskites (*19*) due to quantum confinement effects. Moreover, as compared to lead-salt (LS) materials in which dielectric confinement effects become dominant, they are similar to LS quantum dots (*20*), LS nanorods (*21*) and LS nanosheets (*22*) for similar confinement lengths (see more detailed discussion in section ST1 in the SM and table S2) (*17*). For n=3-5, the exciton binding energy reached a value of ~200 meV, consistent with a system exhibiting 2D quantum confinement, given negligible enhancement of the Coulomb interactions caused by dielectric confinement (*9*). However, in thin films the optical band gap is in a good agreement with that observed for exfoliated crystals for n=1 and 2 but red-shifted by 200 to 300 meV for n=3-5 (Fig. 1G).

We note that the band gap stayed almost constant in thin films with n>2. Any modification to the pristine 2D perovskites phase during thin film fabrication has already been excluded (*11*, *12*). Effects such as changes in dielectric environment and differences in crystallinity (*23*, *24*) cannot account for the redshifts observed in RPP thin films for n>2. The redshifts are also not consistent with electronic impurities at surfaces/interfaces/boundaries in perovskites where carriers are trapped a few tens of millielectron volts within the band gap (*25–28*). Furthermore, optical absorption anisotropy measurements (fig. S5) rule out effects from different orientations of the perovskite layers with respect to light polarization in both thin films and exfoliated crystals (*17*).

We further studied the microscopic origin of the low-energy band gap in thin films for n>2 by confocal spatial mapping (~1 μm resolution) of the PL on a representative n=3 exfoliated crystal (Fig. 2A). Although majority of the basal plane of exfoliated crystal yields spatially homogeneous PL at its band gap energy (2.010 eV), appreciable PL emission was observed from the edges of the exfoliated crystal at 1.680 eV. Figure 2B illustrates the PL spectra of the exfoliated crystal, edges of the exfoliated crystal, and corresponding thin film. The spectra collected at the crystal-edges contain PL peaks observed in both the thin film and exfoliated crystal, which indicates a common origin of the PL from states associated with the edges of the exfoliated crystal (labeled as layer-edge-states, LES) and the PL at low energy in thin films for n>2. Similar results were obtained in the case of n=4 and 5 RPP exfoliated crystals (fig. S6) (*17*), whereas the LES emission was absent when n = 1 or 2.

We probed the spectral origin of the emitting states observed above using PL excitation (PLE) spectroscopy and time-resolved PL (TRPL). The PLE measurements were performed near the edges of the exfoliated crystal in Fig. 2A and revealed both the main exciton emission (labeled X-state) at 2.010 eV and the LES at 1.680 eV. We monitored the PL intensity at the LES energy while sweeping the light-excitation energy between 1.800 and 2.900 eV (Fig. 2C). The PLE showed a clear peak at the position of the exciton (2.010 ± 0.007 eV), but no direct absorption into the LES was observed in the exfoliated crystal (PLE was negligible below 1.900 eV). The spectrum exhibited two high-energy features at ~2.110 eV and 2.200 eV, associated with excited excitonic states and band-to-band absorption, which yielded an exciton binding energy of 200 meV, in agreement with our absorption measurements (Fig. 1E).

These results and the comparable PL intensity of both the X and LES features suggested that part of the photoexcited exciton population decayed to the LES. This mechanism was further validated by probing the TRPL response of both states (Fig. 2D). At short times after the arrival of the light-excitation pulse, the exciton-state became populated over a period of ~100 fs (*25*, *29*) (not resolved here). However, the LES emission reached its maximum PL intensity ~200 ps after the X-state, which is indicative of slow carrier filling from the higher energy exciton to the low-energy edge states. We also observed a nearly four-fold increase in the carrier lifetime of the LES as compared to the exciton, suggesting suppressed nonradiative recombination of the localized carriers. Figure 2E schematically summarizes the photoemission mechanisms in 2D perovskites. The photoexcited exciton diffuses in the perovskite layer emitting a photon at the exciton energy (geminate radiative recombination, see below) or can be quenched via nonradiative recombination. However, these measurements elucidate that, in 2D perovskites with n>2, a part of the photogenerated exciton population travel to the edges of the crystal within its diffusion time, and then undergoes an internal conversion to a LES and efficiently emits photons at a lower energy than the main exciton.

We gained further insight into the physical origin of the optical transitions (Fig. 1, C and D) by analyzing the absorption and photoemission properties of thin films. Figure 3A describes the transitions in thin films with n=3 (fig. S7 for the other n-values) (*17*). The absorption spectrum exhibits resonances at 1.947 ± 0.005, 2.067 ± 0.006, and 2.173 ± 0.006 eV, which are very close in energy to the main exciton-state in exfoliated crystals (2.039 eV). These features

were also observed in the PL spectra at relatively high light-excitation intensity (Fig. 3A, inset), i.e., after saturating the lower-energy LES population. The excitonic nature of these optical resonances was confirmed through (i) linear dependence of the integrated PL signal with respect to the light-excitation intensity I_0 (Fig. 3B, black) and (ii) the negative temperature dependence of their peak energy (figs. S8 and S9) (*5*, *6*, *17*). On the other hand, the main PL peak at 1.695 ± 0.015 eV (Fig. 3A, inset) corresponds to the LES peak observed in exfoliated crystals (Fig. 2B). In sharp contrast to exfoliated crystals (Fig. 2), the PL was dominated by the LES peak, and a broad absorption feature around 1.73 eV (Fig. 3A) accounts for direct absorption into this LES and related mini-bands. These features are a direct consequence of both the light sampling across numerous LES in thin films (Fig. 3D) because of: preferential orientation of perovskite layers normal to the substrate (fig. S10) (*12*, *17*), small grain sizes typically of the order of 200-400 nm (fig. S11) (*12*, *17*), and the relaxation of optical transition selection rules in imperfect crystals.

We also observed that the PL signal associated with the LES varied nonlinearly with the photoexcitation intensity I_0 between 1.30 and 1.45 (Fig. 3B and fig. S7) (*17*). This signal corresponds to a mixed bimolecular and monomolecular recombination of photoexcited carriers (*27*), thus implying a partial dissociation of excitons to free-carrier-like entities as the excitonic states convert (or dissociate) to LES. This conclusion is also consistent with the smooth rise of the absorption at the optical band gap in comparison to the sharp excitonic features observed in exfoliated crystals (Fig. 1, C and E). Moreover, the energy of the LES varied with temperature as 0.21 meV/K (fig. S12) (*17*), which has been attributed in 3D perovskites to the thermal expansion of the lattice where free carriers dominate (*30*). On the contrary, the RPPs with n≤2 that do not exhibit the LES showed negligible or negative temperature dependence of their optical resonances (fig. S8) (*17*), consistent with classical excitonic theory (*5*, *6*).

All of these measurements establish that a different physical origin and behavior of the excitonic and LES features and validated that the main band-gap optical transition in RPP thin films with n>2 originates from the intrinsic electronic structure associated with the edges of the 2D perovskite layers (see discussion in section ST2 in the SM on the possible causes of LES formation) (*17*). Based on our observations, the primary mechanism that emerges in thin films is trapping of the free carriers after exciton dissociation to a deep electronic state located at layer-edges. This model is compatible with both the higher PL efficiency and the longer lifetime of the LES as compared to the higher energy X-states (Fig. 3, B and C). These results imply that, once the carriers are localized at LES, they are protected from non-radiative decay mechanisms such as electron-phonon coupling (*31*, *32*) or electronic impurities (*25*). These key mechanisms of the photoemission in RPPs are captured in Fig. 3E (fig. S13), where, after photogeneration of excitons (left), they can either decay via classical processes (dominant for n≤2, middle) or dissociate to free-carriers potentially trapped at LES (dominant for n>2, right). The process involving intrinsic dissociation of the primary photogenerated excitons to free carrier like states that exist lower in energy in a single-component material is non-intuitive, and not observed in any classical quantum-confined material system.

Motivated by the observed internal exciton dissociation from a part of the higher energy excitonic states to LES that protect the carriers over an appreciably longer timescale, we fabricated high-efficiency PV cells with RPPs and measured their current-voltage (J-V) characteristics and power conversion efficiency (PCE) (Fig. 4, A and B). We observed a sharp break in the current density and PCE from < 2% for n=1 and 2 to >12% for n>2. Assuming comparable charge transport properties for all RPPs, the performance of PV cells for n>2 are impacted by the presence of the LES as: (i) it extends the absorption from the visible to the near infrared, and (ii) it contributes to internal exciton dissociation to free-carrier-like entities that can be more readily collected by the built-in field in a PV device. This was confirmed by measuring the external quantum efficiency (EQE) spectra (Fig. 4C), which showed about five-fold enhancement in collection efficiency in PV cells using RPPs with n>2 as compared to n=1 and 2. Furthermore, the free carriers that converge to the LES remain protected, thus exhibiting long recombination carrier lifetimes resulting in a much higher probability for efficient PL (Fig. 4D and fig. S14) (*17*), which has tremendous implications for high-efficiency light-emitting devices using RPPs with n>2. The variations of the PL efficiency in thin films and of the solar cell efficiency (*33*) between RPPs with n=3,4,5 were possibly due to small variations of the crystal crystallinity and ordering (*12*), and/or light out-coupling and photon recycling effects (*34*). These results pave the path forward for the rational design of high-efficiency optoelectronic devices with solution-processed layered 2D perovskite-based materials.

REFERENCES AND NOTES

1. S. N. Ruddlesden, P. Popper, New compounds of the K_2NiF_4 type. *Acta Crystallogr.* **10**, 538–539 (1957). doi:10.1107/S0365110X57001929
2. S. N. Ruddlesden, P. Popper, The compound $Sr_3Ti_2O_7$ and its structure. *Acta Crystallogr.* **11**, 54–55 (1958). doi:10.1107/S0365110X58000128
3. C. R. Kagan, D. B. Mitzi, C. D. Dimitrakopoulos, Organic-inorganic hybrid materials as semiconducting channels in thin-film field-effect transistors. *Science* **286**, 945–947 (1999). doi:10.1126/science.286.5441.945 Medline
4. C. C. Stoumpos, D. H. Cao, D. J. Clark, J. Young, J. M. Rondinelli, J. I. Jang, J. T. Hupp, M. G. Kanatzidis, Ruddlesden–Popper hybrid lead iodide perovskite 2D homologous semiconductors. *Chem. Mater.* **28**, 2852–2867 (2016). doi:10.1021/acs.chemmater.6b00847

5. T. Ishihara, J. Takahashi, T. Goto, Optical properties due to electronic transitions in two-dimensional semiconductors ($C_nH_{2n+1}NH_3)_2PbI_4$. *Phys. Rev. B* **42**, 11099–11107 (1990). doi:10.1103/PhysRevB.42.11099 Medline
6. N. Kitazawa, M. Aono, Y. Watanabe, Synthesis and luminescence properties of lead-halide based organic-inorganic layered perovskite compounds ($C_nH_{2n+1}NH_3)_2PbI_4$ (n=4, 5, 7, 8 and 9). *J. Phys. Chem. Solids* **72**, 1467–1471 (2011). doi:10.1016/j.jpcs.2011.08.029
7. J. Even, L. Pedesseau, C. Katan, Understanding quantum confinement of charge carriers in layered 2D hybrid perovskites. *ChemPhysChem* **15**, 3733–3741 (2014). doi:10.1002/cphc.201402428 Medline
8. D. Sapori, M. Kepenekian, L. Pedesseau, C. Katan, J. Even, Quantum confinement and dielectric profiles of colloidal nanoplatelets of halide inorganic and hybrid organic-inorganic perovskites. *Nanoscale* **8**, 6369–6378 (2016). doi:10.1039/C5NR07175E Medline
9. L. Pedesseau, D. Sapori, B. Traore, R. Robles, H.-H. Fang, M. A. Loi, H. Tsai, W. Nie, J.-C. Blancon, A. Neukirch, S. Tretiak, A. D. Mohite, C. Katan, J. Even, M. Kepenekian, Advances and promises of layered halide hybrid perovskite semiconductors. *ACS Nano* **10**, 9776–9786 (2016). doi:10.1021/acsnano.6b05944 Medline
10. I. C. Smith, E. T. Hoke, D. Solis-Ibarra, M. D. McGehee, H. I. Karunadasa, A layered hybrid perovskite solar-cell absorber with enhanced moisture stability. *Angew. Chem. Int. Ed.* **53**, 11232–11235 (2014). doi:10.1002/anie.201406466 Medline
11. D. H. Cao, C. C. Stoumpos, O. K. Farha, J. T. Hupp, M. G. Kanatzidis, 2D homologous perovskites as light-absorbing materials for solar cell applications. *J. Am. Chem. Soc.* **137**, 7843–7850 (2015). doi:10.1021/jacs.5b03796 Medline
12. H. Tsai, W. Nie, J.-C. Blancon, C. C. Stoumpos, R. Asadpour, B. Harutyunyan, A. J. Neukirch, R. Verduzco, J. J. Crochet, S. Tretiak, L. Pedesseau, J. Even, M. A. Alam, G. Gupta, J. Lou, P. M. Ajayan, M. J. Bedzyk, M. G. Kanatzidis, A. D. Mohite, High-efficiency two-dimensional Ruddlesden-Popper perovskite solar cells. *Nature* **536**, 312–316 (2016). doi:10.1038/nature18306 Medline
13. K. Tanaka, T. Kondo, Bandgap and exciton binding energies in lead-iodide-based natural quantum-well crystals. *Sci. Technol. Adv. Mater.* **4**, 599–604 (2003). doi:10.1016/j.stam.2003.09.019
14. K. Tanaka, T. Takahashi, T. Kondo, K. Umeda, K. Ema, T. Umebayashi, K. Asai, K. Uchida, N. Miura, Electronic and excitonic structures of inorganic–organic perovskite-type quantum-well crystal ($C_4H_9NH_3)_2PbBr_4$. *Jpn. J. Appl. Phys.* **44**, 5923–5932 (2005). doi:10.1143/JJAP.44.5923
15. K. Gauthron, J.-S. Lauret, L. Doyennette, G. Lanty, A. Al Choueiry, S. J. Zhang, A. Brehier, L. Largeau, O. Mauguin, J. Bloch, E. Deleporte, Optical spectroscopy of two-dimensional layered ($C_{(6)}H_{(5)}C_{(2)}H_{(4)}$-$NH_{(3)})_{(2)}$-$PbI_{(4)}$ perovskite. *Opt. Express* **18**, 5912–5919 (2010). doi:10.1364/OE.18.005912 Medline
16. D. B. Mitzi, K. Chondroudis, C. R. Kagan, Organic-inorganic electronics. *IBM J. Res. Develop.* **45**, 29–45 (2001). doi:10.1147/rd.451.0029
17. Materials and methods are available as supplementary materials.
18. O. Yaffe, A. Chernikov, Z. M. Norman, Y. Zhong, A. Velauthapillai, A. van der Zande, J. S. Owen, T. F. Heinz, Excitons in ultrathin organic-inorganic perovskite crystals. *Phys. Rev. B* **92**, 045414 (2015). doi:10.1103/PhysRevB.92.045414
19. L. M. Herz, Charge-carrier dynamics in organic-inorganic metal halide perovskites. *Annu. Rev. Phys. Chem.* **67**, 65–89 (2016). doi:10.1146/annurev-physchem-040215-112222 Medline
20. J. Jasieniak, M. Califano, S. E. Watkins, Size-dependent valence and conduction band-edge energies of semiconductor nanocrystals. *ACS Nano* **5**, 5888–5902 (2011). doi:10.1021/nn201681s Medline
21. A. C. Bartnik, A. L. Efros, W.-K. Koh, C. B. Murray, F. W. Wise, Electronic states and optical properties of PbSe nanorods and nanowires. *Phys. Rev. B* **82**, 195313 (2010). doi:10.1103/PhysRevB.82.195313
22. J. Yang, F. W. Wise, Electronic states of lead-salt nanosheets. *J. Phys. Chem. C* **119**, 26809–26816 (2015). doi:10.1021/acs.jpcc.5b08207
23. J.-C. Blancon, M. Paillet, H. N. Tran, X. T. Than, S. A. Guebrou, A. Ayari, A. San Miguel, N.-M. Phan, A.-A. Zahab, J.-L. Sauvajol, N. Del Fatti, F. Vallée, Direct measurement of the absolute absorption spectrum of individual semiconducting single-wall carbon nanotubes. *Nat. Commun.* **4**, 2542 (2013). doi:10.1038/ncomms3542 Medline
24. Y. Lin, X. Ling, L. Yu, S. Huang, A. L. Hsu, Y.-H. Lee, J. Kong, M. S. Dresselhaus, T. Palacios, Dielectric screening of excitons and trions in single-layer MoS_2. *Nano Lett.* **14**, 5569–5576 (2014). doi:10.1021/nl501988y Medline
25. X. Wu, M. T. Trinh, D. Niesner, H. Zhu, Z. Norman, J. S. Owen, O. Yaffe, B. J. Kudisch, X.-Y. Zhu, Trap states in lead iodide perovskites. *J. Am. Chem. Soc.* **137**, 2089–2096 (2015). doi:10.1021/ja512833n Medline
26. W. Nie, H. Tsai, R. Asadpour, J.-C. Blancon, A. J. Neukirch, G. Gupta, J. J. Crochet, M. Chhowalla, S. Tretiak, M. A. Alam, H.-L. Wang, A. D. Mohite, Solar cells. High-efficiency solution-processed perovskite solar cells with millimeter-scale grains. *Science* **347**, 522–525 (2015). doi:10.1126/science.aaa0472 Medline
27. J.-C. Blancon, W. Nie, A. J. Neukirch, G. Gupta, S. Tretiak, L. Cognet, A. D. Mohite, J. J. Crochet, The effects of electronic impurities and electron–hole recombination dynamics on large-grain organic–inorganic perovskite photovoltaic efficiencies. *Adv. Funct. Mater.* **26**, 4283–4292 (2016). doi:10.1002/adfm.201505324
28. D. W. de Quilettes, S. M. Vorpahl, S. D. Stranks, H. Nagaoka, G. E. Eperon, M. E. Ziffer, H. J. Snaith, D. S. Ginger, Solar cells. Impact of microstructure on local carrier lifetime in perovskite solar cells. *Science* **348**, 683–686 (2015). doi:10.1126/science.aaa5333 Medline
29. K. Abdel-Baki, F. Boitier, H. Diab, G. Lanty, K. Jemli, F. Lédée, D. Garrot, E. Deleporte, J. S. Lauret, Exciton dynamics and non-linearities in two-dimensional hybrid organic perovskites. *J. Appl. Phys.* **119**, 064301 (2016). doi:10.1063/1.4941345
30. H. Wang, L. Whittaker-Brooks, G. R. Fleming, Exciton and free charge dynamics of methylammonium lead iodide perovskites are different in the tetragonal and orthorhombic phases. *J. Phys. Chem. C* **119**, 19590–19595 (2015). doi:10.1021/acs.jpcc.5b04403
31. Z. Guo, X. Wu, T. Zhu, X. Zhu, L. Huang, Electron–phonon scattering in atomically thin 2D perovskites. *ACS Nano* **10**, 9992–9998 (2016). doi:10.1021/acsnano.6b04265 Medline
32. D. B. Straus, S. Hurtado Parra, N. Iotov, J. Gebhardt, A. M. Rappe, J. E. Subotnik, J. M. Kikkawa, C. R. Kagan, Direct observation of electron–phonon coupling and slow vibrational relaxation in organic–inorganic hybrid perovskites. *J. Am. Chem. Soc.* **138**, 13798–13801 (2016). doi:10.1021/jacs.6b08175 Medline
33. O. D. Miller, E. Yablonovitch, S. R. Kurtz, Strong internal and external luminescence as solar cells approach the Shockley-Queisser limit. *IEEE J. Photovolt.* **2**, 303–311 (2012). doi:10.1109/JPHOTOV.2012.2198434
34. J. M. Richter, M. Abdi-Jalebi, A. Sadhanala, M. Tabachnyk, J. P. H. Rivett, L. M. Pazos-Outón, K. C. Gödel, M. Price, F. Deschler, R. H. Friend, Enhancing photoluminescence yields in lead halide perovskites by photon recycling and light out-coupling. *Nat. Commun.* **7**, 13941 (2016). doi:10.1038/ncomms13941 Medline
35. J. C. de Mello, H. F. Wittmann, R. H. Friend, An improved experimental determination of external photoluminescence quantum efficiency. *Adv. Mater.* **9**, 230–232 (1997). doi:10.1002/adma.19970090308
36. N. Sestu, M. Cadelano, V. Sarritzu, F. Chen, D. Marongiu, R. Piras, M. Mainas, F. Quochi, M. Saba, A. Mura, G. Bongiovanni, Absorption F-sum rule for the exciton binding energy in methylammonium lead halide perovskites. *J. Phys. Chem. Lett.* **6**, 4566–4572 (2015). doi:10.1021/acs.jpclett.5b02099 Medline
37. A. Miyata, A. Mitioglu, P. Plochocka, O. Portugall, J. T.-W. Wang, S. D. Stranks, H. J. Snaith, R. J. Nicholas, Direct measurement of the exciton binding energy and effective masses for charge carriers in organic-inorganic tri-halide perovskites. *Nat. Phys.* **11**, 582–587 (2015). doi:10.1038/nphys3357
38. J. Even, L. Pedesseau, C. Katan, Analysis of multivalley and multibandgap absorption and enhancement of free carriers related to exciton screening in hybrid perovskites. *J. Phys. Chem. C* **118**, 11566–11572 (2014). doi:10.1021/jp503337a
39. R. L. Milot, R. J. Sutton, G. E. Eperon, A. A. Haghighirad, J. Martinez Hardigree, L. Miranda, H. J. Snaith, M. B. Johnston, L. M. Herz, Charge-carrier dynamics in 2D hybrid metal–halide perovskites. *Nano Lett.* **16**, 7001–7007 (2016). doi:10.1021/acs.nanolett.6b03114 Medline
40. H.-H. Fang, F. Wang, S. Adjokatse, N. Zhao, M. A. Loi, Photoluminescence enhancement in formamidinium lead iodide thin films. *Adv. Funct. Mater.* **26**, 4653–4659 (2016). doi:10.1002/adfm.201600715

ACKNOWLEDGMENTS

The work at Los Alamos National Laboratory (LANL) was supported by LANL LDRD program (J-C.B., W.N., S.T., A.D.M.) and was partially performed at the Center for Nonlinear Studies. The work was conducted, in part, at the Center for Integrated Nanotechnologies (CINT), a U.S. Department of Energy, Office of Science user facility. Work at Northwestern University was supported by grant SC0012541 from the U.S. Department of Energy, Office of Science. The work in France was supported by Cellule Energie du CNRS (SOLHYBTRANS Project) and University of Rennes 1 (Action Incitative, Défis Scientifique Emergents 2015). This research used resources of the Center for Functional Nanomaterials, which is a U.S. DOE Office of Science Facility, at Brookhaven National Laboratory under Contract No. DE-SC0012704. Author contributions: J.C.B, A.D.M and J.J.C. conceived the idea, designed the experiments, and wrote the manuscript. H.T. and W.N. fabricated thin-films and performed all device measurements and analysis. J.E, C.K. and S.T. analyzed the data and performed HSE calculations with support from M.K. and L.P. and provided insight into the mechanisms. M.G.K., C.S.S. and C.M.M.S. developed the chemistry for the synthesis of phase-pure crystals and provided insight into the chemical origin of the edge states. M.S. and K.A. performed several complementary measurements to provide insight into the mechanisms and to validate the observed findings. P.M.A. provided insights into the origin of edge states. All authors contributed to this work, read the manuscript and agree to its contents, and all data are reported in the main text and supplemental materials.

SUPPLEMENTARY MATERIALS

www.sciencemag.org/cgi/content/full/science.aal4211/DC1
Materials and Methods
Supplementary Text
Figures S1 to S14
Tables S1 and S2
References (*35*–*40*)

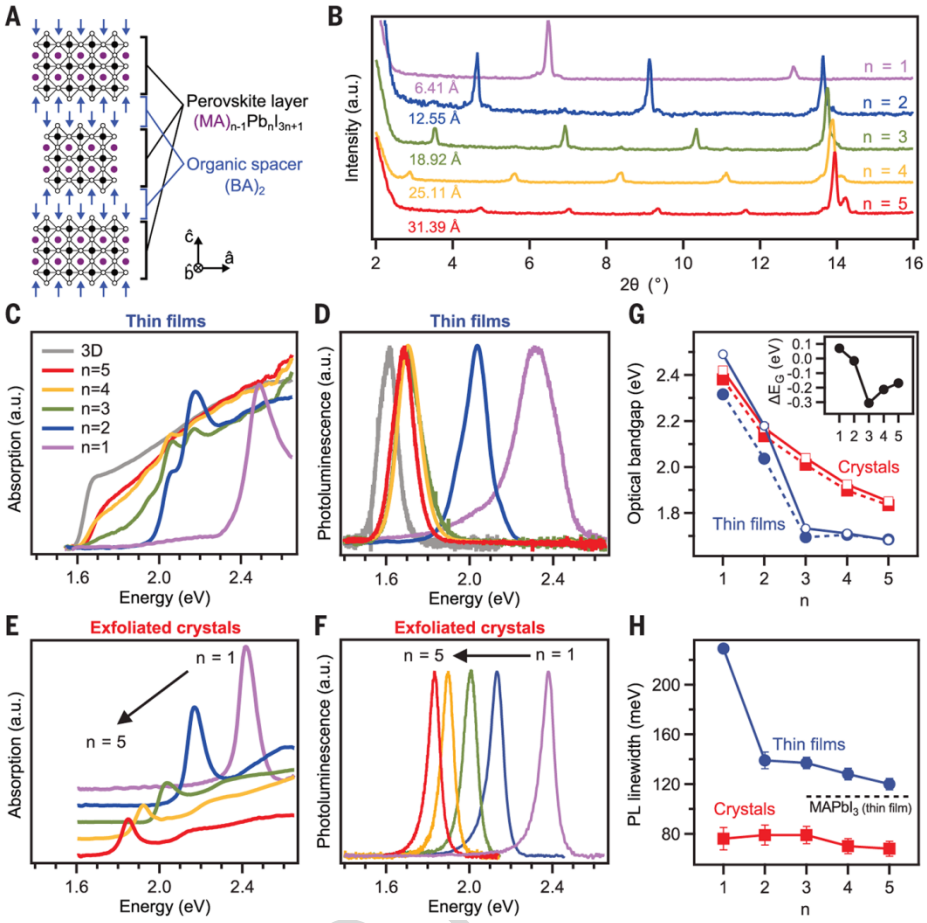

Fig. 1. Evidence of phase-purity of the RPPs (n=1 to 5) and comparison of optical properties of thin films and exfoliated crystals. (**A**) Schematics of the QW like crystal structure showing perovskite layers in the plane ($\hat{a},\hat{b}$) sandwiched between organic spacing layers. (**B**) Phase purity established by monitoring the position and number of the low angle peaks in x-ray diffraction patterns for each n-value. Absorption and photoluminescence (PL) of the thin films (**C**) and (**D**) and exfoliated crystals (**E**) and (**F**). (**G**) Optical band gap derived from absorption (open symbols) and PL (full symbols) as a function of n. (inset) Shift of the optical band gap in thin films with respect to exfoliated crystals (from absorption). (**H**) PL linewidth versus n showing inhomogeneous broadening in thin films as compared to exfoliated crystals.

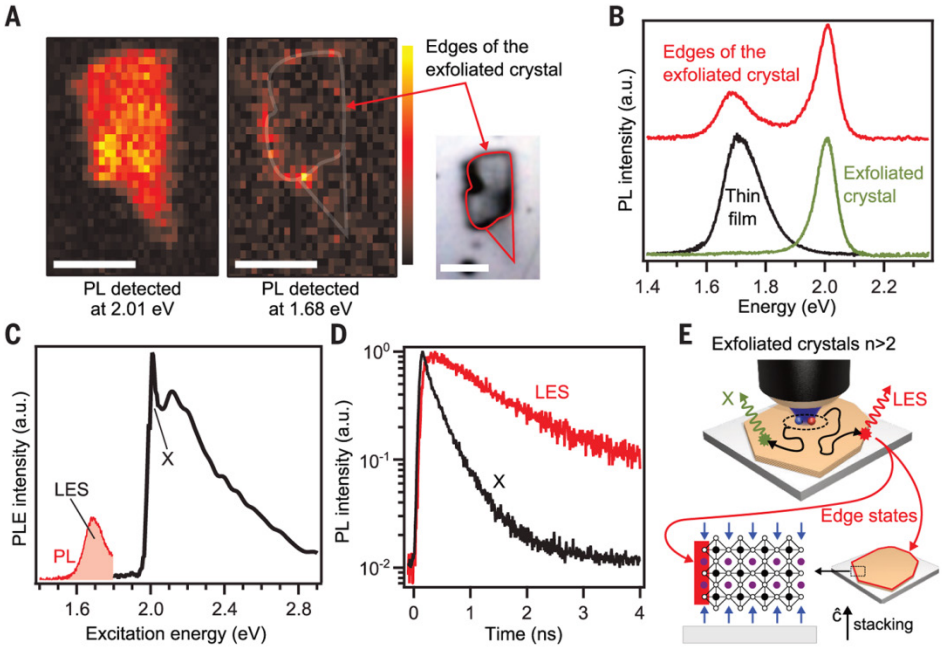

Fig. 2. Microscopic origin of the low-energy band gap in 2D perovskite thin films for n=3. (**A**) PL intensity map of a single exfoliated crystal, probed at 2.010 eV and 1.680 eV. (Right) Microscopy image showing the layer edges of the exfoliated crystal. Scale bar is 10 μm. (**B**) Comparison of the PL in the exfoliated crystal, at the exfoliated crystal edges, and in the corresponding thin film. (**C**) PLE integrated signal of the LES, measured by locally exciting the exfoliated crystal edges. The measured PL profile of the LES is also plotted. (**D**) TRPL of the PL features X and LES observed in (B) and (C). (**E**) Schematics of the photo-absorption and PL processes in 2D perovskite exfoliated crystals with n>2.

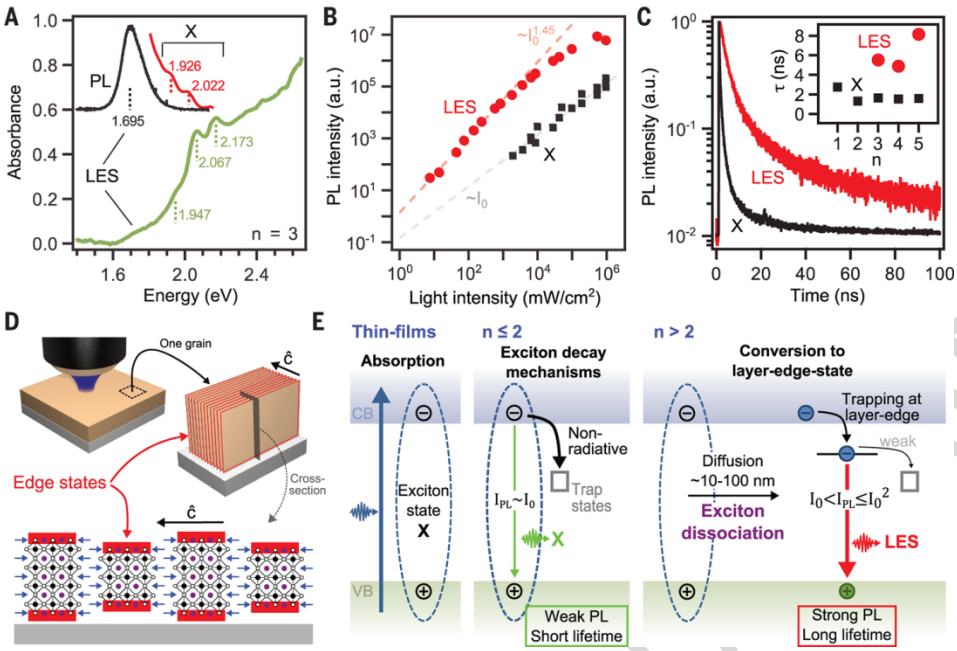

Fig. 3. Optical absorption and emission mechanisms in thin films of 2D perovskites. (**A**) Thin film n=3 absorption (green), PL at photo-excitation 100 mW/cm^2 (black) and 10^6 mW/cm^2 (red). (**B**) Light-excitation intensity (I_0) dependence of the integrated PL. Dashed lines are fits to the data. (**C**) TRPL in the thin films n=3. (Inset) Corresponding lifetimes of the X-states and LES as a function of the n-value. Excitation at ~100 mW/cm^2. (**D**) Schematics of the photo-absorption and PL processes in a 2D perovskite thin film with n>2. In contrast to exfoliated crystals, thin film perovskite layers are preferentially oriented normal to the substrate (fig. S10) (*12*, *17*), therefore excitation light probes numerous amount of LES. (**E**) Summary of the main photoemission mechanisms in thin films. The diffusion length was estimated from fig. S13 (*17*).

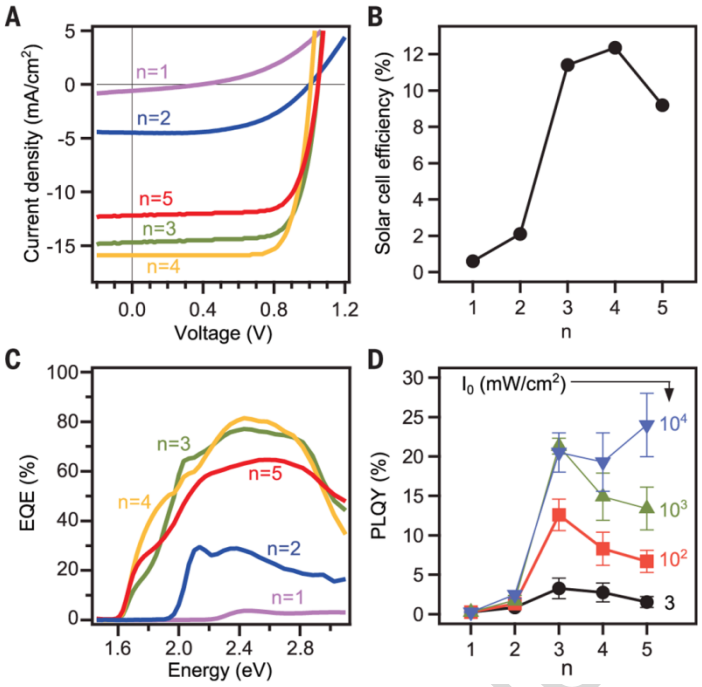

Fig. 4. Figures of merit of thin film devices for light-harvesting and solid-state emission. (**A**) J-V characteristics measured under AM1.5 illumination. (**B**) Power conversion efficiency as a function of 2D perovskite n-value (QW thickness). (**C**) External quantum efficiency for the PV devices in A. (**D**) PL quantum yield (PLQY) in thin films as a function of n-value for several light excitation intensity.